Photon-number-resolved asymmetric dissociative single ionization of H_2

Wenbin Zhang,[1] Hui Li,[1] Kang Lin,[1] Peifen Lu,[1] Xiaochun Gong,[1] Qiying Song,[1] Qinying Ji,[1] Junyang Ma,[1] Hanxiao Li,[1] Heping Zeng,[1] Feng He,[2] and Jian Wu[1,3,*]

[1]*State Key Laboratory of Precision Spectroscopy, East China Normal University, Shanghai 200062, China*

[2]*Key Laboratory of Laser Plasmas (Ministry of Education) and School of Physics and Astronomy, Collaborative Innovation Center for IFSA (CICIFSA), Shanghai Jiao Tong University, Shanghai 200240, China*

[3]*Collaborative Innovation Center of Extreme Optics, Shanxi University, Taiyuan, Shanxi 030006, China*

(Received 9 June 2017; published 7 September 2017)

The electron-nuclear joint energy spectrum allows one to unambiguously count the total number of photons absorbed by the electrons and nuclei of a molecule. Driven by phase-controlled, linearly polarized two-color femtosecond laser pulses, we experimentally demonstrate that the asymmetric bond breaking of a singly ionized H_2 depends on the total number of photons absorbed by the molecule in the ionization and dissociation processes. The accessibilities of different dissociation pathways and their interference-induced asymmetric electron localization as a function of the absorbed photons are retrieved. Our results strengthen the understanding of the directional bond breaking of a molecule from the aspect of the correlated electron-nuclear dynamics.

DOI: 10.1103/PhysRevA.96.033405

I. INTRODUCTION

Directional molecular bond breaking induced by asymmetric dissociative ionization has attracted enormous attention for its important implications in coherent manipulation of chemical reactions [1–3]. Driven by asymmetric laser fields produced by carrier-envelope-phase stabilized few-cycle [4–10] or phase-controlled two-color femtosecond pulses [11–19], the dissociative single ionization of a molecule generally proceeds in two steps. In the first step, an electron is liberated and a nuclear wave packet (NWP) on the ground cationic state is launched. In the second step, the created NWP dissociates into neutral and charged fragments assisted by photon-coupled resonant transitions among various electronic states. Since the ionization step is symmetric for homonuclear diatomic molecules, e.g., H_2 and its isotopes [20–24], the coherent superposition of the dissociated NWPs of same final kinetic energy but opposite parities leads to the observed asymmetric emission of the ionic fragment along the field polarization. Recently, two-dimensional directional dissociative single ionization of H_2 was observed in phase-controlled polarization-gated two-color laser fields [17,19]. In addition to the laser-induced coupling of various electronic states in the dissociation step, it was demonstrated that the selective ionization governed by the orbital shape of spatially orientated molecules [25–30], the laser-phase-dependent electron recollision [31], and the laser-induced coupling of vibrational wave packets [32–35] also contribute to the directional bond breaking of molecules.

When exposed to a strong laser field, the electrons and nuclei of a molecule as a whole absorb multiple photons in the ionization and dissociation steps. As compared to the atoms, the electrons and nuclei of a molecule share the absorbed photon energy [36–45], i.e., the photon energy is correlatively partitioned between electrons and nuclei. Until now, the role of the photon energy sharing between the electron and nuclei on directional breaking of molecules has not been explicitly explored, in particular, the dependence on the total number of the photons absorbed by the molecule in the ionization and dissociation processes.

In this paper, we report the experimental observation of directional dissociative single ionization of H_2 as a function of the total number of photons absorbed by the molecule. The joint energy spectrum (JES) of the coincidently measured electron and nuclei is employed to count the total number of photons absorbed by the molecule in the ionization and dissociation processes. Phase-controlled linearly polarized two-color femtosecond laser pulses are utilized to drive the directional bond breaking. Our results show that the dissociation pathways producing high nuclear energy become accessible with increased proportions when more photons are absorbed by the molecule. The change of the relative weight of different dissociation pathways alters the asymmetry of the observed directional breaking of the molecule.

II. EXPERIMENTAL SETUP

Experimentally, as depicted in Fig. 1, the phase-controlled linearly polarized two-color laser field was produced in a phase-locked Mach-Zehnder interferometer. The linearly polarized fundamental wave (FW) pulse (25 fs, 790 nm, 10 kHz) derived from a multipass Ti:sapphire amplifier is down-collimated into a 150-μm-thick β-barium borate (β-BBO) crystal to generate a second harmonic (SH) pulse centered at 395 nm. Two dichroic mirrors are used to separate, and later recombine the FW and SH pulses. A half-wave plate is placed in the FW arm to rotate its polarization to be parallel to that of the SH pulse (along the z axis). The temporal overlap of the two pulses is controlled by a motorized delay stage in the FW arm. To finely tune the relative phase, denoted as ϕ_L, between the two colors and meanwhile to overcome the ineluctable fluctuation of the relative optical path length between the FW and SH arms due to the air flow and/or mechanical vibration, a phase-locked system based on the spatial interference of a reference continuum-wave (cw) laser at 532 nm is employed [19,46]. The phase-controlled, linearly polarized two-color pulse is then tightly focused onto a supersonic gas jet of H_2 by a concave silver mirror

*jwu@phy.ecnu.edu.cn

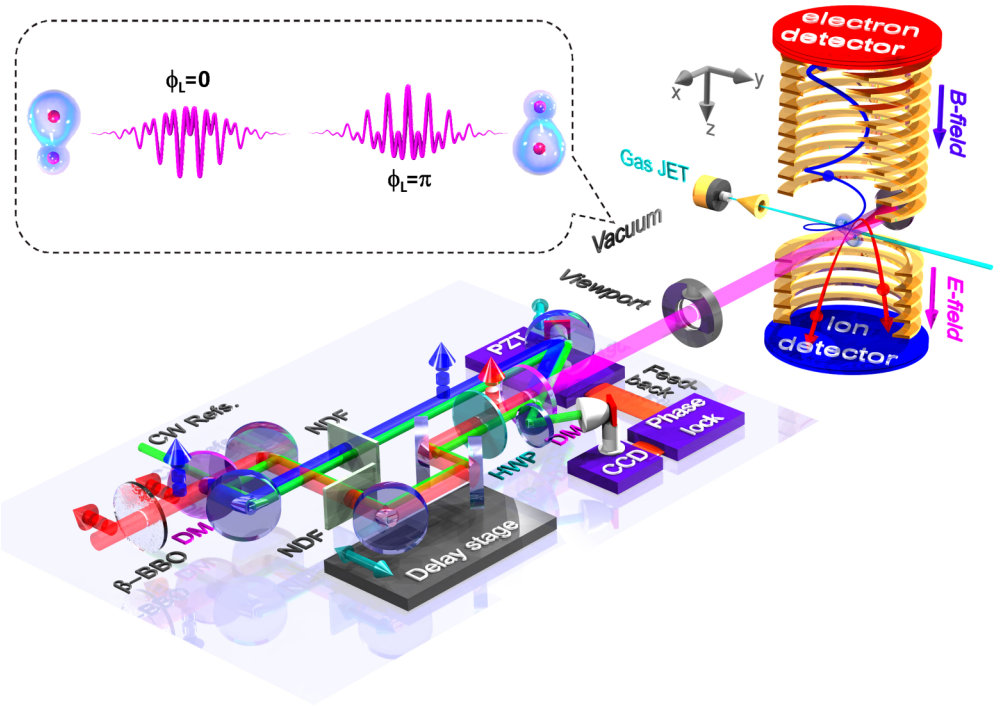

FIG. 1. Schematic diagram of the experimental apparatus. The red and blue arrows stand for the polarization of the FW and SH components of the two-color field. HWP: half-wave plate, DM: dichroic mirror, NDF: neutral density filter. The inset illustrates that the remaining electron can localize at one of the nuclei depending on the phase of the two-color field in the dissociative single ionization of H_2.

($f = 7.5$ cm) inside an ultrahigh vacuum chamber of the cold-target recoil-ion momentum spectroscopy (COLTRIMS) apparatus [47,48]. The photoionization-created ions and electrons are guided by a weak homogenous electric field and magnetic field which are eventually detected in coincidence by two time- and position-sensitive microchannel plate detectors at the opposite ends of the spectrometer. The three-dimensional momenta of the detected ions and electrons are retrieved from the measured times-of-flight and positions of the impacts during the offline analysis. The field intensities of the FW and SH pulses in the interaction region are calibrated individually by blocking one of the two pulses before the dichroic beam combiner of the Mach-Zehnder interferometer. By examining the proton spectrum [49] or tracing the field-intensity-dependent shift of the discrete above threshold ionization spectrum [50] of H_2, the laser intensities of the FW and SH pulses are estimated to be $I_{FW} \approx 1.2\times10^{13}$ W/cm^2 and $I_{SH} \approx 3.3\times10^{13}$ W/cm^2, respectively.

III. RESULTS AND DISCUSSIONS

To reveal the directional molecular bond breaking driven by two-color laser fields, we focus on the multiphoton dissociative single ionization channel of $H_2 + m\hbar\omega \rightarrow H^+ + H + e^-$, hereafter denoted as the $H_2(1,0)$ channel. As schematically illustrated in Fig. 2(a), by absorbing multiple photons from the two-color fields, the neutral H_2 molecule emits one electron and launches a NWP on the $1s\sigma_g{}^+$ state of $H_2{}^+$. The created NWP then starts to move along the potential curves of $H_2{}^+$, which may be coupled back and forth between the $1s\sigma_g{}^+$ and $2p\sigma_u{}^+$ states when the energy gap matches certain photon energies, e.g., $1\omega_{FW}$, $1\omega_{SH}$, or $3\omega_{FW}$. The molecular ion eventually dissociates into H and H^+ along the $1s\sigma_g{}^+$ and $2p\sigma_u{}^+$ states. Due to the coherent superposition of the NWPs of the same final kinetic energy but opposite parities dissociated from the $1s\sigma_g{}^+$ and $2p\sigma_u{}^+$ states [4–17], the electron asymmetrically localizes on the nuclei. For quantification, we define the asymmetry parameter as

$$A(E_N,\phi_L) = [Y(E_N,\phi_L) - Y(E_N,\phi_L+\pi)]/ [Y(E_N,\phi_L) + Y(E_N,\phi_L+\pi)], \quad (1)$$

where $Y(E_N,\phi_L)$ is the H^+ yield at kinetic energy E_N and laser phase ϕ_L. The asymmetry parameter A is positive for electron localization on the down nucleus and negative on the other site, as illustrated in Fig. 2(a). Here, E_N is the total kinetic energy of the ejected proton and the neutral fragment, i.e., $E_N = E_{H^+} + E_H$. The kinetic energy of the neutral H atom (not detectable in our present experiment) is deduced based on the momentum conservation of the ejected fragments from the breaking molecule. The absolute value of ϕ_L is calibrated by observing the phase-dependent directional dissociative double ionization of CO molecules [15,27].

Figure 2(b) displays the two-dimensional (2D) asymmetry spectrum as a function of ϕ_L and E_N obtained by integrating over all the electron energy E_e. The corresponding E_N spectrum is plotted in Fig. 2(c). The asymmetric dissociative ionization of molecules can be contributed by the interference of various pathways accessed by absorbing and emitting different numbers of photons in the dissociation process [23], as illustrated in Fig. 2(a). As demonstrated in previous studies on the asymmetric dissociative single ionization of hydrogen molecules by two-color laser fields [14–17,19], there are several dissociation pathways with overlapped

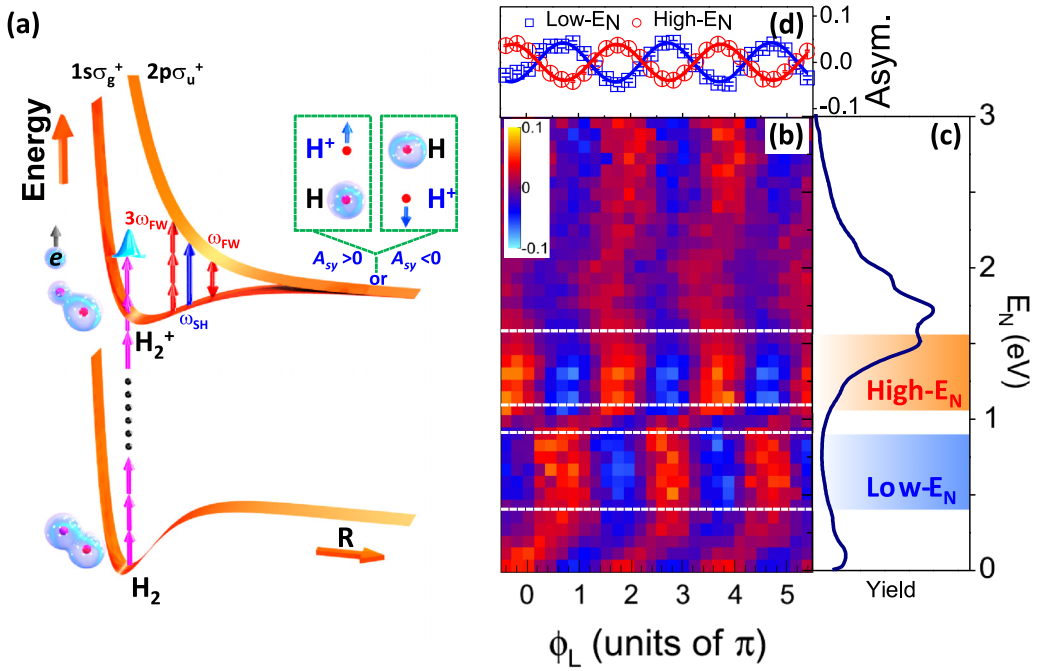

FIG. 2. (a) Schematic illustration of the multiphoton dissociative single ionization of H_2 driven by a two-color laser pulse. A NWP on the $1s\sigma_g^+$ state of H_2^+ is launched by releasing one electron from H_2 in the ionization step. The created NWP afterwards propagates on the potential curves of H_2^+ and asymmetrically dissociates into a neutral H and an ionic H^+ after conclusion of the two-color laser pulse, assisted by photon-coupled transitions among the $1s\sigma_g^+$ and $2p\sigma_u^+$ states. The schematic potential curves of neutral H_2 and ionic H_2^+ are adopted from Refs. [51] and [52]. (b) Measured two-dimensional spectrum of the asymmetry parameter as a function of the laser phase ϕ_L and the kinetic energy of the nuclei E_N. (c) Measured phase-averaged E_N spectrum. (d) Asymmetry parameters of the low-E_N (0.4 eV $< E_N <$ 0.9 eV) and high-E_N (1.1 eV $< E_N <$ 1.6 eV) regions as indicated between the white dashed lines in (b). The solid sinusoidal curves are the numerical fits of the measured data.

kinetic energies, e.g., $1\omega_{SH}$-$1\omega_{FW}$, $1\omega_{FW}$, net-$2\omega_{FW}$, $1\omega_{SH}$, $1\omega_{SH}+2\omega_{FW}-1\omega_{FW}$, and $3\omega_{FW}$ pathways, may contribute to the interference and lead to the observed asymmetries at different energies of the E_N spectrum.

For the energy region of $0\,\text{eV} < E_N < 1.0\,\text{eV}$, the $1\omega_{SH}$-$1\omega_{FW}$ pathway (propagation on the $1s\sigma_g^+$ state undergoes one-ω_{SH}-photon coupled transition to the $2p\sigma_u^+$ state, followed by propagation on the $2p\sigma_u^+$ state and coupling back to the $1s\sigma_g^+$ state, by emitting one ω_{FW} photon, followed by dissociating along the $1s\sigma_g^+$ state) and $1\omega_{FW}$ pathway (propagation on the $1s\sigma_g^+$ state undergoes one-ω_{FW}-photon coupled transition to the $2p\sigma_u^+$ state, followed by dissociating along the $2p\sigma_u^+$ state) are involved. Meanwhile, the ionization-created NWP may directly dissociate along the $1s\sigma_g^+$ state without additional photon-coupled transition to the $2p\sigma_u^+$ state, i.e., a zero-photon dissociation pathway [8,9], which will carry only very limited kinetic energy. On the other hand, the net-$2\omega_{FW}$ pathway (propagation on the $1s\sigma_g^+$ state undergoes a three-ω_{FW}-photon transition to the $2p\sigma_u^+$ state, followed by propagation on the $2p\sigma_u^+$ state and coupling back to the $1s\sigma_g^+$ state by emitting one ω_{FW} photon, followed by dissociating along the $1s\sigma_g^+$ state) and $1\omega_{SH}$ pathway (propagation on the $1s\sigma_g^+$ state undergoes one-ω_{SH}-photon coupled transition to the $2p\sigma_u^+$ state, followed by dissociating along the $2p\sigma_u^+$ state) would contribute to the interference in the energy region of $1.0\,\text{eV} < E_N < 2.0\,\text{eV}$. For the energy region of $E_N > 2.0\,\text{eV}$, the observed asymmetry might arise from the interference between the $1\omega_{SH}+2\omega_{FW}-1\omega_{FW}$ pathway (propagation on the $1s\sigma_g^+$ state undergoes transition to the $2p\sigma_u^+$ state by absorbing one ω_{SH} and two ω_{FW} photons, followed by propagation on the $2p\sigma_u^+$ state and coupling back to the $1s\sigma_g^+$ state by emitting one ω_{FW} photon, followed by dissociating along the $1s\sigma_g^+$ state) and $3\omega_{FW}$ pathway (propagation on the $1s\sigma_g^+$ state undergoes three-ω_{FW}-photon transition to the $2p\sigma_u^+$ state, followed by dissociating along the $2p\sigma_u^+$ state). In our following discussions we mainly focus on the energy regions of $0.4\,\text{eV} < E_N < 0.9\,\text{eV}$ (denoted as low E_N) and $1.1\,\text{eV} < E_N < 1.6\,\text{eV}$ (denoted as high E_N) as marked in Fig. 2(c). The observed asymmetries of the proton emission in the low- and high-E_N regions originate from the interference between the $1\omega_{FW}$ and $1\omega_{SH}$-$1\omega_{FW}$ pathways, and between the $1\omega_{SH}$ and net-$2\omega_{FW}$ pathways, respectively. As shown in Fig. 2(d), the low- and high-E_N regions exhibit different dependences on the laser phase due to the participation of different pathways. The solid curves are the numerical fits of the measured data by using $A = A_0\cos(\phi_L+\varphi_{A0})$, where A_0 and φ_{A0} are the amplitude and phase offset of the asymmetry parameter, respectively.

We will now discuss the dependence of the asymmetry parameter on the total number of photons absorbed by the molecule in the multiphoton ionization and dissociation processes. To unambiguously count the total number of photons absorbed by the molecule in the ionization and dissociation steps, the electron-nuclear JES is employed. As compared to atoms, the multiphoton above threshold ionization (ATI)

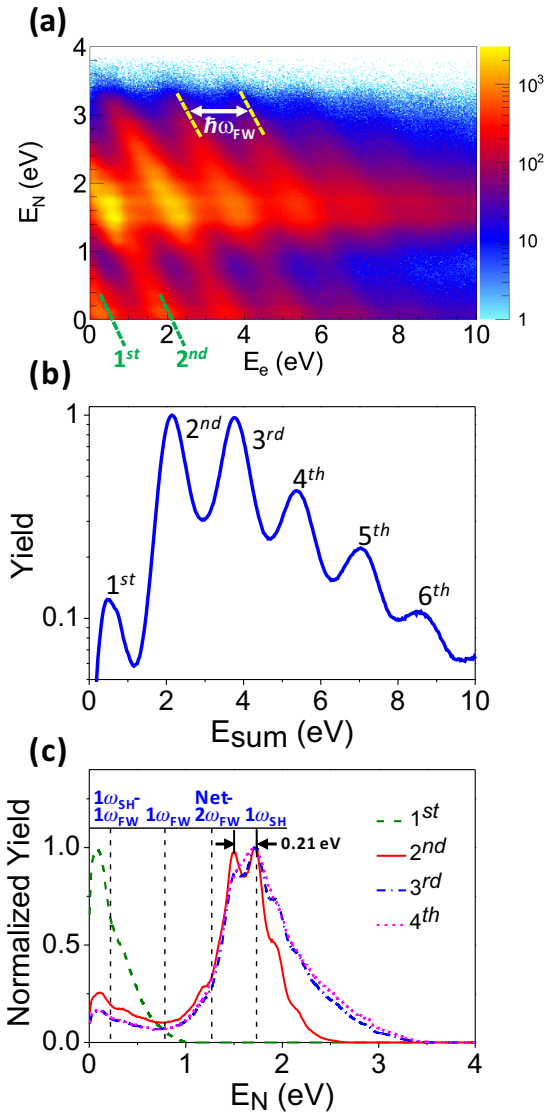

FIG. 3. (a) Measured electron-nuclear JES of the $H_2(1,0)$ channel. (b) The corresponding sum energy E_{sum} of the ejected electron and nuclear fragments from a single molecule. Each peak in the E_{sum} spectrum stands for a diagonal line in the JES spectrum in (a) as indicated by the numbers. (c) The normalized E_N distributions integrated over E_e for the first four diagonal energy conservation lines in (a). The expected location of the E_N for four dissociation pathways mentioned in the text are marked by the dashed lines.

of the molecules may produce discrete diagonal lines in the JES as a consequence of the correlated sharing of the absorbed photon energy above the ionization threshold among the outgoing electron and nuclear fragments [36–45]. Each diagonal line indicates that the molecule as a whole absorbs a constant number of photons, i.e., the sum energy of the ejected electron and nuclear fragments $E_{sum} = E_N + E_e = m\hbar\omega - (I_{p0} + U_p)$. Here I_{p0} is the ionization threshold, U_p is the ponderomotive energy, and m is the number of absorbed photons by the molecule. The measured ϕ_L-integrated electron-nuclear JES of the $H_2(1,0)$ channel driven by the two-color pulse is shown in Fig. 3(a). Multiple diagonal lines spaced by the photon energy of the FW field ($\hbar\omega_{FW}$) are clearly observed in the JES. They correspond to the discrete ATI peaks in the E_{sum} spectrum as shown in Fig. 3(b), where each peak stands for one diagonal line in the JES. For a given energy conservation line in Fig. 3(a), the electron energy E_e decreases with the increase of the nuclear energy E_N, since their sum E_{sum} is a constant. Thus, the total energy absorbed by the molecule can be revealed by counting the diagonal lines in the electron-nuclear JES or the discrete peaks in the E_{sum} spectrum.

By counting the number of photons absorbed by the molecule, one can trace the accessibility of various pathways of the dissociative ionization. Figure 3(c) shows the normalized E_N spectrum integrated over E_e for the first four diagonal lines in Fig. 3(a), which is equivalent to the first four discrete ATI peaks in Fig. 3(b). The locations of the expected E_N peak for the four dissociation pathways mentioned above, i.e., $1\omega_{SH}$-$1\omega_{FW}$ (~0.23 eV), $1\omega_{FW}$ (~0.78 eV), net-$2\omega_{FW}$ (~1.27 eV), and $1\omega_{SH}$ (~1.73 eV) pathways, are indicated by the vertical dashed lines in Fig. 3(c), respectively. The expected final kinetic energy of the nuclei for different dissociation pathways is estimated by assuming that the launched NWP is at rest when it propagates to the internuclear distance for the first photon-resonant transition between the $1s\sigma_g{}^+$ and $2p\sigma_u{}^+$ states. The discrete fine subfeatures at around 1.7 eV of the E_N spectra in Fig. 3(c) or the diagonal lines of the JES in Fig. 3(a) indicate the participation of the vibrational states of the ground cation state of $H_2{}^+$ (e.g., $E_{v=5} - E_{v=4} \approx 0.21$ eV of the $1s\sigma_g{}^+$ state). The visibility of the subfeatures decreases for high ATI orders due to the limited statistics of our measurements.

More interestingly, for each diagonal line of the JES or the ATI peak of the E_{sum} spectrum, the corresponding E_N spectrum reveals the relative weight of different dissociation pathways when a certain number of photons are absorbed by the molecule. For instance, the E_N spectrum is dominated by the $1\omega_{SH}$-$1\omega_{FW}$ pathway for the first ATI order, while for the second and higher orders, other dissociation pathways, e.g., $1\omega_{FW}$, net-$2\omega_{FW}$, and $1\omega_{SH}$, become accessible with increased proportions. This is because with more photons absorbed by the molecule, more energies would deposit into the nuclei, and the channel opening of the dissociation pathways with higher final kinetic energies can be initialized. The relative yields of the different pathways and thus the ultimate asymmetric breaking of the molecule induced by their interference depend on the number of absorbed photons.

Figure 4(a) displays the numerically fitted amplitudes A_0 of the asymmetry parameters for various ATI peaks of the low- and high-E_N regions, respectively. The amplitude of the asymmetry increases with the increase of the ATI order. For the interference of various pathways with opposite parities, the amplitude A_0 of the observed asymmetry is governed by the relative yield (R) of the involved interfering pathways, which is related to the laser phase of the two-color pulse and the number of the absorbed photons. According to the semiclassical model proposed in Ref. [53], the expected asymmetry parameter for the interference can be expressed as $A_c = [2R/(R^2+1)]\cos(\Delta\varphi)$. By assuming that the amplitude of the asymmetry parameter of the semiclassical model equals A_0 of the fitting function, i.e., $2R/(R^2+1) = A_0$, we can deduce the relative weight R between different dissociation pathways, i.e., $1\omega_{FW}$ and $1\omega_{SH}$-$1\omega_{FW}$ pathways, and the $1\omega_{SH}$

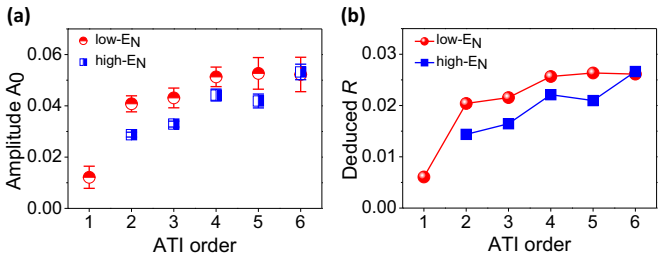

FIG. 4. (a) Fitted asymmetry amplitude A_0 of the $H_2(1,0)$ channel in low-E_N (red circles) and high-E_N (blue squares) regions as a function of the ATI order of the E_{sum} spectrum. (b) Deduced relative weight (R) of various dissociation pathways as a function of ATI order of the E_{sum} spectrum.

and net-$2\omega_{FW}$ pathways for the low- and high-E_N regions, respectively. As shown in Fig. 4(b), the deduced relative weight R between the dissociation pathways involved in the interference increases with the increasing ATI order. For high ATI orders, since the molecule absorbs many photons from the laser fields and all the possible dissociation channels are accessed with almost constant probability, the relative weight of various pathway tends to be invariable.

IV. CONCLUSION

In summary, we experimentally investigate the asymmetric dissociative single ionization of H_2 in phase-controlled, linearly polarized two-color femtosecond laser pulses by counting the total number of photons absorbed by the molecule. The electrons and nuclei of the molecule as a whole absorb the photon energy in the ionization and dissociation steps, which can be revealed by the JES or the sum energy of the electron and nuclear fragments ejected from a single molecule measured in coincidence. Our results allow us to trace the accessibility of various dissociation pathways and their interference-induced asymmetric bond breaking as a function of the total number of photons absorbed by the molecule from the aspect of the correlated electron-nuclear dynamics.

ACKNOWLEDGMENTS

This work is supported by the National Natural Science Fund (Grants No. 11425416, No. 11621404, No. 11574205, and No. 11322438), the 111 project of China (Grant No. B12024), the Shanghai Sailing Program (Grant No. 17YF1404000), and the Outstanding Doctoral Dissertation Cultivation Plan of Action (Grant No. YB2016036).

[1] A. H. Zewail, Science **242**, 1645 (1988).
[2] A. Assion, T. Baumert, M. Bergt, T. Brixner, B. Kiefer, V. Seyfried, M. Strehle, and G. Gerber, Science **282**, 919 (1998).
[3] A. S. Alnaser and I. V. Litvinyuk, J. Phys. B **50**, 032002 (2017).
[4] M. F. Kling, Ch. Siedschlag, A. J. Verhoef, J. I. Khan, M. Schultze, Th. Uphues, Y. Ni, M. Uiberacker, M. Drescher, F. Krausz, and M. J. J. Vrakking, Science **312**, 246 (2006).
[5] M. Kremer, B. Fischer, B. Feuerstein, V. L. B. de Jesus, V. Sharma, C. Hofrichter, A. Rudenko, U. Thumm, C. D. Schröter, R. Moshammer, and J. Ullrich, Phys. Rev. Lett. **103**, 213003 (2009).
[6] B. Fischer, M. Kremer, T. Pfeifer, B. Feuerstein, V. Sharma, U. Thumm, C. D. Schröter, R. Moshammer, and J. Ullrich, Phys. Rev. Lett. **105**, 223001 (2010).
[7] I. Znakovskaya, P. von den Hoff, G. Marcus, S. Zherebtsov, B. Bergues, X. Gu, Y. Deng, M. J. J. Vrakking, R. Kienberger, F. Krausz, R. de Vivie-Riedle, and M. F. Kling, Phys. Rev. Lett. **108**, 063002 (2012).
[8] T. Rathje, A. M. Sayler, S. Zeng, P. Wustelt, H. Figger, B. D. Esry, and G. G. Paulus, Phys. Rev. Lett. **111**, 093002 (2013).
[9] N. G. Kling, K. J. Betsch, M. Zohrabi, S. Zeng, F. Anis, U. Ablikim, B. Jochim, Z. Wang, M. Kübel, M. F. Kling, K. D. Carnes, B. D. Esry, and I. Ben-Itzhak, Phys. Rev. Lett. **111**, 163004 (2013).
[10] H. Xu, T. Y. Xu, F. He, D. Kielpinski, R. T. Sang, and I. V. Litvinyuk, Phys. Rev. A **89**, 041403(R) (2014).
[11] E. Charron, A. Giusti-Suzor, and F. H. Mies, Phys. Rev. Lett. **71**, 692 (1993).
[12] B. Sheehy, B. Walker, and L. F. DiMauro, Phys. Rev. Lett. **74**, 4799 (1995).
[13] H. Ohmura, N. Saito, and M. Tachiya, Phys. Rev. Lett. **96**, 173001 (2006).
[14] D. Ray, F. He, S. De, W. Cao, H. Mashiko, P. Ranitovic, K. P. Singh, I. Znakovskaya, U. Thumm, G. G. Paulus, M. F. Kling, I. V. Litvinyuk, and C. L. Cocke, Phys. Rev. Lett. **103**, 223201 (2009).
[15] J. Wu, A. Vredenborg, L. Ph. H. Schmidt, T. Jahnke, A. Czasch, and R. Dörner, Phys. Rev. A **87**, 023406 (2013).
[16] V. Wanie, H. Ibrahim, S. Beaulieu, N. Thiré, B. E. Schmidt, Y. Deng, A. S. Alnaser, I. V. Litvinyuk, X. Tong, and F. Légaré, J. Phys. B **49**, 025601 (2016).
[17] X. Gong, P. He, Q. Song, Q. Ji, H. Pan, J. Ding, F. He, H. Zeng, and J. Wu, Phys. Rev. Lett. **113**, 203001 (2014).
[18] Q. Song, X. Gong, Q. Ji, K. Lin, H. Pan, J. Ding, H. Zeng, and J. Wu, J. Phys. B **48**, 094007 (2015).
[19] K. Lin, X. Gong, Q. Song, Q. Ji, W. Zhang, J. Ma, P. Lu, H. Pan, J. Ding, H. Zeng, and J. Wu, J. Phys. B **49**, 025603 (2016).
[20] A. D. Bandrauk, S. Chelkowski, and H. S. Nguyen, Int. J. Quantum Chem. **100**, 834 (2004).
[21] X. M. Tong and C. D. Lin, Phys. Rev. Lett. **98**, 123002 (2007).
[22] F. He, C. Ruiz, and A. Becker, Phys. Rev. Lett. **99**, 083002 (2007).
[23] V. Roudnev and B. D. Esry, Phys. Rev. Lett. **99**, 220406 (2007).
[24] F. Kelkensberg, G. Sansone, M. Y. Ivanov, and M. Vrakking, Phys. Chem. Chem. Phys. **13**, 8647 (2011).
[25] S. De, I. Znakovskaya, D. Ray, F. Anis, N. G. Johnson, I. A. Bocharova, M. Magrakvelidze, B. D. Esry, C. L. Cocke, I. V. Litvinyuk, and M. F. Kling, Phys. Rev. Lett. **103**, 153002 (2009); **112**, 159902 (2014).
[26] I. Znakovskaya, P. von den Hoff, S. Zherebtsov, A. Wirth, O. Herrwerth, M. J. J. Vrakking, R. de Vivie-Riedle, and M. F. Kling, Phys. Rev. Lett. **103**, 103002 (2009).

[27] H. Li, D. Ray, S. De, I. Znakovskaya, W. Cao, G. Laurent, Z. Wang, M. F. Kling, A. T. Le, and C. L. Cocke, Phys. Rev. A **84**, 043429 (2011).
[28] I. Znakovskaya, P. Von den Hoff, N. Schirmel, G. Urbasch, S. Zherebtsov, B. Bergues, R. de Vivie-Riedle, K. M. Weitzel, and M. F. Kling, Phys. Chem. Chem. Phys. **13**, 8653 (2011).
[29] J. Wu, L. Ph. H. Schmidt, M. Kunitski, M. Meckel, S. Voss, H. Sann, H. Kim, T. Jahnke, A. Czasch, and R. Dörner, Phys. Rev. Lett. **108**, 183001 (2012).
[30] K. J. Betsch, N. G. Johnson, B. Bergues, M. Kubel, O. Herrwerth, A. Senftleben, I. Ben-Itzhak, G. G. Paulus, R. Moshammer, J. Ullrich, M. F. Kling, and R. R. Jones, Phys. Rev. A **86**, 063403 (2012).
[31] X. Xie, K. Doblhoff-Dier, S. Roither, M. S. Schöffler, D. Kartashov, H. Xu, T. Rathje, G. G. Paulus, A. Baltuska, S. Gräfe, and M. Kitzler, Phys. Rev. Lett. **109**, 243001 (2012).
[32] E. Wells, C. E. Rallis, M. Zohrabi, R. Siemering, B. Jochim, P. R. Andrews, U. Ablikim, B. Gaire, S. De, K. D. Carnes, B. Bergues, R. de Vivie-Riedle, M. F. Kling, and I. Ben-Itzhak, Nat. Commun. **4**, 2895 (2013).
[33] M. Kübel, R. Siemering, C. Burger, N. G. Kling, H. Li, A. S. Alnaser, B. Bergues, S. Zherebtsov, A. M. Azzeer, I. Ben-Itzhak, R. Moshammer, R. de Vivie-Riedle, and M. F. Kling, Phys. Rev. Lett. **116**, 193001 (2016).
[34] A. S. Alnaser, M. Kübel, R. Siemering, B. Bergues, N. G. Kling, K. J. Betsch, Y. Deng, J. Schmidt, Z. A. Alahmed, A. M. Azzeer, J. Ullrich, I. Ben-Itzhak, R. Moshammer, U. Kleineberg, F. Krausz, R. de Vivie-Riedle, and M. F. Kling, Nat. Commun. **5**, 3800 (2014).
[35] H. Li, N. G. Kling, B. Förg, J. Stierle, A. Kessel, S. A. Trushin, M. F. Kling, and S. Kaziannis, Struct. Dyn. **3**, 043206 (2016).
[36] C. B. Madsen, F. Anis, L. B. Madsen, and B. D. Esry, Phys. Rev. Lett. **109**, 163003 (2012).
[37] R. E. F. Silva, F. Catoire, P. Rivière, H. Bachau, and F. Martín, Phys. Rev. Lett. **110**, 113001 (2013).
[38] J. Wu, M. Kunitski, M. Pitzer, F. Trinter, L. Ph. H. Schmidt, T. Jahnke, M. Magrakvelidze, C. B. Madsen, L. B. Madsen, U. Thumm, and R. Dörner, Phys. Rev. Lett. **111**, 023002 (2013).
[39] L. Yue and L. B. Madsen, Phys. Rev. A **88**, 063420 (2013).
[40] K. L. Liu, P. F. Lan, C. Huang, Q. B. Zhang, and P. X. Lu, Phys. Rev. A **89**, 053423 (2014).
[41] F. Catoire, R. E. F. Silva, P. Rivière, H. Bachau, and F. Martín, Phys. Rev. A **89**, 023415 (2014).
[42] V. Mosert and D. Bauer, Phys. Rev. A **92**, 043414 (2015).
[43] W. Zhang, Z. Li, P. Lu, X. Gong, Q. Song, Q. Ji, K. Lin, J. Ma, F. He, H. Zeng, and J. Wu, Phys. Rev. Lett. **117**, 103002 (2016).
[44] X. Sun, M. Li, Y. Shao, M.-M. Liu, X. Xie, Y. Deng, C. Wu, Q. Gong, and Y. Liu, Phys. Rev. A **94**, 013425 (2016).
[45] P. Lu, W. Zhang, X. Gong, Q. Song, K. Lin, Q. Ji, J. Ma, F. He, H. Zeng, and J. Wu, Phys. Rev. A **95**, 033404 (2017).
[46] M. Chini, H. Mashiko, H. Wang, S. Chen, C. Yun, S. Scott, S. Gilbertson, and Z. Chang, Opt. Express **17**, 21459 (2009).
[47] R. Dörner, V. Mergel, O. Jagutzki, L. Spielberger, J. Ullrich, R. Moshammer, and H. Schmidt-Böcking, Phys. Rep. **330**, 95 (2000).
[48] J. Ullrich, R. Moshammer, A. Dorn, R. Dörner, L. P. H. Schmidt, and H. Schmidt-Böcking, Rep. Prog. Phys. **66**, 1463 (2003).
[49] A. S. Alnaser, X. M. Tong, T. Osipov, S. Voss, C. M. Maharjan, B. Shan, Z. Chang, and C. L. Cocke, Phys. Rev. A **70**, 023413 (2004).
[50] K. Henrichs, M. Waitz, F. Trinter, H. Kim, A. Menssen, H. Gassert, H. Sann, T. Jahnke, J. Wu, M. Pitzer, M. Richter, M. S. Schöffler, M. Kunitski, and R. Dörner, Phys. Rev. Lett. **111**, 113003 (2013).
[51] B. D. Esry and H. R. Sadeghpour, Phys. Rev. A **60**, 3604 (1999).
[52] J. McKenna, F. Anis, A. M. Sayler, B. Gaire, N. G. Johnson, E. Parke, K. D. Carnes, B. D. Esry, and I. Ben-Itzhak, Phys. Rev. A **85**, 023405 (2012).
[53] J. Wu, M. Magrakvelidze, L. P. H. Schmidt, M. Kunitski, T. Pfeifer, M. Schöffler, M. Pitzer, M. Richter, S. Voss, H. Sann, H. Kim, J. Lower, T. Jahnke, A. Czasch, U. Thumm, and R. Dörner, Nat. Commun. **4**, 2177 (2013).